Research Square

Preprints are preliminary reports that have not undergone peer review.
They should not be considered conclusive, used to inform clinical practice,
or referenced by the media as validated information.

Imaging of different crustal and mantle discontinuities below the Hyderabad, Eastern Dharwar Craton, India

Prantik Mandal (prantikmandal62@gmail.com)
CSIR-National Geophysical Research Institute
Sandeep Gupta
CSIR-National Geophysical Research Institute
K. Sivaram
CSIR-National Geophysical Research Institute
Sanjay Kumar
CSIR-National Geophysical Research Institute
Sudesh Kumar
CSIR-National Geophysical Research Institute
Rahul Biswas
CSIR-National Geophysical Research Institute
Raju Prathigada
CSIR-National Geophysical Research Institute
B. N.V Prasad
CSIR-National Geophysical Research Institute
M. Saidixit
CSIR-National Geophysical Research Institute

Research Article

Keywords: Radial P-Receiver Functions, Dharwar Craton, S-wave Velocity Structure, Moho Depth, Lithospheric thickness

Posted Date: July 27th, 2022

DOI: https://doi.org/10.21203/rs.3.rs-1873167/v1

License: This work is licensed under a Creative Commons Attribution 4.0 International License.
Read Full License

Abstract

To monitor seismicity, a 10-station broadband seismic network was deployed in the Hyderabad region by CSIR-NGRI, Hyderabad, India, during 2020-21. The analysis of radial P receiver functions using data from this network detects conversions from five major crustal and mantle discontinuities below the region. Our CCP stacking of radial PRFs also images the nature and geometry of these seismic discontinuities viz., Moho (increase in positive amplitude at 30–40 km depths), Hales discontinuity (increase in positive amplitude at 90–120 km depths), lithosphere-asthenosphere boundary (LAB) (increase in negative amplitude at 130–160 km depths), 410-km (increase in positive PRF amplitude at 410–440 km depths) and 660-km (increase in positive PRF amplitude at 620–660 km depths). Our modeling also reveals that the mean depth to the Moho, Hales discontinuity and LAB below the study region are 36, 115 and 160 km, respectively, suggesting the absence of a thick cratonic root below the EDC. We also model the differential time of the 410-km and 660-km conversions, which is found to be 24 s at most of the stations that is the same as the theoretical differential time between these two phases according to the IASP91 global reference velocity model, indicating a typical cratonic behaviour of the EDC. However, a noticeable upward movement of the 410-km discontinuity and a slight downward movement of the 660-km discontinuity below the central part of the study region is also modelled that suggests a thickening of the Mantle transition zone, which could be attributed to the presence of probable imprints of the Archean subduction below the Hyderabad, EDC, India.

1. Introduction

Detection of the crustal and Mantle discontinuities in terms of sudden changes in seismic velocities and density values along the interfaces below any region has been a prime objective of the seismological research (O'Reilly and Griffin, 2013; Bina, 1991; Fisher et al., 2010; Shearer, 2000). The geometry and nature of these discontinuities provide important information about the geodynamic processes, which were responsible for shaping the complex geology of any region. The crust-mantle boundary, lithosphere-asthenosphere boundary, mantle transition zone, core –mantle boundary and inner-outer core boundary are found to be associated with large changes in velocity and density, which are known as the first-order discontinuities in the interior of the Earth (O'Reilly and Griffin, 2013; Bina, 1991; Fisher et al., 2010; Shearer, 2000). Besides there are some second order discontinuities like Conrad discontinuity, Hale's discontinuity, 220-km discontinuity and 670 km discontinuity (Lawry, 1997; Hales, 1969; Shearer, 2019), which are observed to be associated with smaller changes in seismic velocities and density. It has been observed that first order discontinuities are found everywhere in the world while second order discontinuities are observed only in some parts of the world (Shearer, 2019). Stacking and analysis of different conversions on the radial receiver functions have been widely used to detect the above-mentioned discontinuities inside the Earth (Kiselev et al., 2008; Saul et al., 2000).

Until today, many investigators have tried to delineate the crustal and mantle structure below the 3.6 Ga Dharwar craton, which revealed marked lateral variations in the crustal and lithospheric structure across the craton (e.g. ~38–54 km and 160–210 km in WDC (western Dharwar craton), ~ 32–38 km and 130–

170 km in EDC (eastern Dharwar craton)) (Kiselev et al., 2008; Singh et al., 2015; Borah et al., 2015; Kumar et al., 2001; Sarkar et al., 2003; Saha et al., 2020). The Moho depths and crustal composition below the Hyderabad region, which is located on the EDC, have been modelled to be 30.5–36.0 km and 0.24–0.26, respectively (Gaur and Priestley, 1997; Rai et al., 2003; Saul et al., 2000; Zhou et al., 2000). Besides, Kiselev et al. (2008) and Saul et al. (2000) have also detected a weak positive Hales discontinuity at 80–90 km depth below Hyderabad, 120 km below the WDC and 100 km below the EDC (Kiselev et al., 2008). The evidence of Hales discontinuity has also been detected at a few locations in India by a P-receiver function study (Jagadeesh and Rai, 2008). The Hales discontinuity associated with an increase in S-wave velocity at 80–90 km in USA was first observed by Hales in 1969. This increase in Vs has been attributed to the presence of anisotropy or partial melts in mantle olivine. Further, the presence of mantle discontinuities at 410 and 660 km depths, representing top and bottom layers of the mantle transition zone (MTZ), has also been modelled below the Dharwar craton using receiver function studies (Kiselev et al., 2008; Lessing et al., 2014). The 410 and 660 km discontinuities in India have been mapped using PP and SS reflections at 410–440 km and 660 km, respectively (Lessing et al., 2014). It is a well-established fact that the differential time between P660s and P410s is always close to 23.9 s (Chevrot et al., 1999; Kumar and Mohan, 2005). According to the IASP91 velocity model, theoretical arrival times of P410s and P660s conversions are 44 and 68 s, respectively. Kiselev et al. (2008) have reported that P410s and P660s phases have arrived at their respective standard arrival times according to a homogeneous flat earth model, suggesting the presence of smaller variations in the MTZ thickness below the Dharwar craton.

Here we present modelled geometry and nature of different crustal and mantle discontinuities below the Hyderabad region on the EDC, through the analysis and Common Conversion Point (CCP) stacking of radial P-receiver functions. The broadband waveform data of 49 good teleseismic events (during October 2020 – December 2021) from a seismic network of 10 three-component broadband seismographs in and around Hyderabad region has been utilized for the present study (Figs. 1a-c; Mandal et al., 2022). Here we present the analysis of different conversions from the different crustal and mantle discontinuities. We also construct Common Conversion Point (CCP) images of radial PRFs below the region showing different major seismic discontinuities viz., Moho, Hales discontinuity, lithosphere-asthenosphere boundary and Mantle transition zone. Finally, the modelled crustal and mantle structure has been interpreted in terms of geodynamic processes responsible for shaping the complex geology of the region.

2. Seismic Network

A seismic network of 10 three-component broadband seismographs was installed by CSIR-NGRI, Hyderabad, in the Hyderabad and surrounding regions, from September 2020 to December 2021. Each station was equipped with a 24-bit Nanometrics Data Acquisition system and a Trillium (nat. period 120 s) broadband sensor. The time tagging was done by a GPS receiver at each station resulting in accuracy in microseconds. The data was recorded continuously 100 samples per second, which resulted in picking of P- and S- phases with an accuracy of 0.01s. Using the data from the above network, 60 local events were located using the P- and S- arrival times, and in-built location programs of the SEISAN software

(Ottemoller et al., 2018). The initial locations of these events were having RMS error of the order of 0.05 s, resulting in mean epicentral location error of 1 km and mean focal depth error of 2.0 km. The epicentres of the located events clustered around already mapped lineaments/faults in Hyderabad (Fig. 1a). The focal depths of these events have been modelled to vary from surface to a depth of about 40 km (Fig. 1c).

3. Data And Methods

Here, for the present study, we used three component digital waveforms of 49 good teleseismic earthquakes (out of 127 good recorded teleseismic events) of M_w5.5-7.1, with a high signal-to-noise ratio (SNR > 2) and clear P-arrivals. These selected events are having with back azimuth between 22° and 341°, epicentres between 32.5°S and 89.6°N, and ray parameters ranging from 0.042 to 0.078 s/km (Fig. 1b). We used a P-wave window from − 5 and 60 s from the three-component broadband waveforms, which are corrected from the instrumental response that is done through the transfer command of SAC software using the poles and zeros information. Then, the NS and EW horizontal components were rotated using back-azimuth to calculate radial (R) and transverse components (T). Subsequently, the radial PRFs are computed by deconvolving Z-component from the R-componnet in the time domain while transverse PRFs are computed by deconvolving Z-component from the T-component in the time domain. All the windowed waveforms are filtered using a high pass filter with a corner frequency of 0.02 Hz before the computation of PRFs. Here, the iterative time-domain deconvolution procedure of Ligorria and Ammon (1999) with 200 iterations is used to compute radial and transverse PRFs for each event, using Gaussian width factor (a) = 2.5 (f < 1.25 Hz), where f marks the corner frequency of a low-pass filter. Thus, for an average crustal shear velocity of 3.5 km/s. the wavelength would be 4.4 km for f = 1.25. Thus, the calculated PRFs with a = 2.5 can resolve layers with a thickness of 2.2 km, respectively. Finally, we select those deconvolutions that reproduced more than 90% of the signal energy on the radial component (when convolved back with the vertical trace).

4. Analysis Of Different Conversions On The Radial Prfs

Here for the PRF computation, we analyse broadband data of 490 three-component waveforms from ten broadband stations (Fig. 1a). First, we study a total of 490 individual radial RFs from all ten stations as a function of horizontal slowness (Fig. 2). Note that each individual, gather and stacked radial PRF shows clear, sharp and positive P-to-S conversion (P_M at 4.0-4.6 s after Pp (i.e., direct P arrival)) associated with the Moho boundary (M), a positive conversion associated with the Hale's discontinuity (P_H at 9–13 s after Pp)), a negative P-to-S conversion (P_L at 17-19.5 s after Pp) associated with the Lithosphere-Asthenosphere boundary (LAB), and conversions associated with the upper (P_{410-km} at 410-km) and lower (P_{660-km} at 660-km) boundary of the Mantle transition zone (Figs. 2–5). Figures 2,4 show distinct arrivals of P_M, P_H, and P_L on the individual and stacked radial PRFs at all the selected 10 stations. Figures 3–4 (also see Supplementary Figs. S2-S6) show clear arrivals of all the above-mentioned crustal and Mantle conversions on the individual, stacked and gather radial PRFs at all 10 stations (Table 1).

Subsequently, we model the geometry and nature of these crustal and mantle discontinuities beneath the study area, through the CCP stacking of radial PRFs along the four profiles striking SN, WE, NW-SE, and SW-NE (Figs. 6a-b and 7a-b). The 2-D PRF stacked images along the above-mentioned profiles reveal clear images of Moho, Hale's discontinuity, LAB, 410-km boundary and 660-km boundary, which do not show any noticeable variations in the Moho depths(Figs. 6a-b, 7a-b). However, we notice some variations in Hale's discontinuity, LAB, 410-km and 660-km discontinuities, below the region.

4.1 Common Conversion Point (CCP) stacking of radial PRFs

In this paper, the CCP imaging of radial PRFs has been performed using the Funclab software (Eagar, 2012). Following Dueker and Sheehan (1997)'s methodology, this software generates a 2-D image of impedance contrast at depth, through coherently stacking P-to-S phase conversions on the radial PRFs. The details of CCP imaging methodology have been discussed in Cladwell et al. (2013) and the manual of Funclab (Eagar, 2012)). Here, we used the 1-D IASP91 velocity model for the CCP imaging (Kennett and Engdahl, 1991)). We have performed CCP imaging along four profiles (NS striking A1A2, WE striking B1B2, NW-SE trending C1C2 and SW-NE trending D1D2), whose locations are shown in Fig. 1a. The results of CCP stacking of radial PRFs along A1A2, B1B2, C1C2 and D1D2 profiles are shown in Figs. 6a-b and 7a-b.

We compute PRFs using one frequency bands corresponding to Gaussian width factor, a = 2.5 (f < 1.25 Hz), where "f" marks the corner frequency of a low-pass filter. Thus, the wavelength would be 3.2 km for f = 1.25, for an average crustal shear velocity of 4.0 km/s. Thus, the calculated PRFs with a = 2.5 can resolve layers with a thickness of 1.6 km. The nominal vertical resolution at the Moho could be 4 km for the 1-D PRFs and 1.7 km for the 2-D CCP stack (Cladwell et al., 2013). While the horizontal resolution depends on the Fresnel zone. The Fresnel zone width for Ps at 40 km is ~ 40 km. The station spacing for our stations varies from 10 to 20 km. So our station spacing of ~ 20 km could yield 50% overlap at 40 km depth, which is found to be sufficient to image the Moho well (Cladwell et al., 2013). At 10 km depth, the Frensel zone width is 20 km, which could be an image with 50% overlap for our stations with a 10 km spacing. But, our station spacing could not provide a better resolution for images at depths less than 10 km.

5. Results And Discussions

We model nature and geometry of crustal and mantle discontinuities at 10 broadband stations through the analysis and CCP stacking of radial PRFs. From individual radial PRFs (Figs. 2a-j) and staked as well as gather radial PRFs (Figs. 4–5), the positive arrivals of P_M and P_H conversions are modelled to range from 3.9 to 4.5 s and from 11.5 to 15 s, respectively (Table 1), suggesting Moho depths ranging from 31 to 36 km (by assuming a Pn velocity of 8 km/s) and depths to the Hale's discontinuity varying from 92 to 120 km. While the sharp negative arrivals from the LAB (P_L) range from 17 to 19 s after the direct P,

indicating lithospheric thicknesses varying from 144 to 162 km (assuming Vp in upper mantle is 8.5 km/s). We also generated a ray plot between piercing points of PRFs and station locations, which clearly shows three discontinuities i.e. Moho (increase in PRF amplitudes at ~ 32–37 km), Hales (increase in PRF amplitudes at ~ 90–125 km) and LAB (decrease in PRF amplitudes at ~ 130–160 km) below the region (see Supplementary Fig. S1).

Most interestingly, we note that the differential time of the 410-km and 660-km conversions at most of the stations is found to be 24 s (Table 1), which is the same as the theoretical differential time between these two phases according to the IASP91 velocity model (Kennet and Engdahl, 1991). This observation suggests that variations in 410-km and 660-km boundaries are not significant below the region, which is in agreement with the modelling results of Kiselev et al. (2008). However, we notice marked upward movement in the 410-km discontinuity below the central portion of the C1C2 and D1D2 profiles (Figs. 7a-b), suggesting a slight thickening of the MHT below the region. This slight thickening of the MTZ could be attributed to the presence of probable imprints of the Archean subduction below the Hyderabad region as proposed by Pahari et al. (2020) based on petrochemical studies of Hyderabad granites.

Depth-wise migrated stacked radial PRFs at 10 broadband stations (Figs. 5a-b) reveal that the average depth to Moho boundary, Hale's discontinuity and lithosphere-asthenosphere boundary below the region are modelled to be 36, 115 and 160 km, respectively. It will be worth to discuss the existing depth estimates of the Moho, Hale's discontinuity, and lithosphere-asthenosphere boundary for the Dharwar craton here. Note that earlier seismological studies using modelling of surface waves, ambient noise, and P- as well as S- receiver functions have shown a variation in Moho depths between 32–38 km in EDC (e.g. ~38–54 km in WDC, ~ 32–38 km in EDC and ~ 40–46 km in SGT) (Kiselev et al., 2008; Singh et al., 2015; Borah et al., 2015; Kumar et al., 2001; Sarkar et al., 2003; Rychert and Harmon, 2016). The depths of the Hale's discontinuity has been modelled to be varying from 80 to 120 km below the Dharwar craton from the earlier seismological studies (Saul et al., 2000; Jagadeesh and Rai, 2008; Kiselev et al., 2008). The thickness of seismological lithosphere in the Dharwar craton has been found to be varying from 100 to 250 km (Srinagesh et al., 1989; Polet and Anderson, 1995; Gupta et al., 2003; Jagadeesh and Rai, 2008). However, a thinner lithosphere of 80–100 km in the Dharwar Craton has been modelled through S-RF study (Kumar et al., 2007). But, another S-RF study has depicted a lithospheric thickness of 150–210 km in the EDC (Ramesh et al., 2010). The thickness of the thermal lithosphere in the southern Indian craton has been modelled to be varying from 80 to 250 km (Pandey and Agarwal, 1999; Negi et al., 1986; Gupta et al., 1991). The modelling of magneto-telluric data in the Dharwar craton has shown that the thickness of the conductive lithosphere varies from 80 to > 200 km (Gokarn et al., 2004; Patro and Sarma, 2009; Naganjaneyulu and Santosh, 2011). Further, a lithospheric thickness of 160–250 km has been inferred for the Dharwar craton from the modelling of Kimberlite xenoliths geochemical data (Ganguly and Bhattacharya 1987; Griffin et al., 2009). Thus, our estimates of mean depths to the Moho, Hale's discontinuities and lithosphere-asthenosphere boundary are agreeing well with the above-discussed available estimates of M, H and L in the EDC.

Our CCP stacking of radial PRFs along the SN striking A1A2, WE striking B1B2, NW-SE trending C1C2 and SW-NE trending D1D2 profiles have clearly mapped the lateral variations in depths of Moho, Hales discontinuity, LAB and MTZ across the region (Figs. 6a-b and 7a-b). The 2-D images along the A1A2 (SN striking) and B1B2 (WE striking) profiles delineate no remarkable lateral variations in the crustal-mantle (M), LAB (L), 410-km and 660-km boundaries except some small changes in the Hale's discontinuity (H) is noticed below the central part of the A1A2 and B1B2 profiles. The PRF imaging along the NW-SE striking C1C2 and SW-NE striking D1D2 profiles reveal almost no lateral variation in the Moho depths while H and L boundaries suggest small variations below the eastern part of the study area (i.e. NE and SE parts of C1C2 and D1D2 profiles) where noticeable changes in 410-km and 660-km boundaries are also noted. Interestingly, Figs. 6a-b showing depth cross-sections along NS and EW profiles suggest a flat nature of 410-km and 660-km discontinuity below the region. Whilst Fig. 7a-b showing depth cross-sections along the NW-SE (i.e. C1C2) and SW-NE (i.e. D1D2) profiles detect a zone of slight thickening of the MHT (as shown by the red dotted rectangular zones), suggesting the presence of probable imprints of the Archean subduction as also suggested by Pahari et al. (2020) based on petrochemical studies of Hyderabad granites. Most interestingly, 2-D images along all the above-mentioned four profiles very distinctly detect five major discontinuities below the region viz. Moho (increase in positive PRF amplitude at 30–40 km depths), Hales discontinuity (increase in positive PRF amplitude at 90–115 km depths), LAB (increase in negative PRF amplitude at 130–160 km depths), 410-km boundary (increase in positive PRF amplitude at 410–460 km depths) and 660-km boundary (increase in positive PRF amplitude at 640–660 km depths) (Figs. 6a-b and 7a-b). We also note that these images also suggest an almost flat Moho but they do show some undulations on the Hales discontinuity and LAB. Most interestingly, our modelled depths to Hales discontinuity (i.e. 90–125 km depths) and lithosphere-asthenosphere boundary (i.e. 130–160 km depths) are agreeing well with the available depth estimates of these discontinuities in the Dharwar craton from other studies (Saul et al., 2000; Jagadeesh and Rai, 2008; Kiselev et al., 2008).

7. Conclusions

We have imaged nature and geometry of different crustal and mantle discontinuities underlying the Hyderabad and its neighbouring regions through analysis of individual, stacked and gather radial PRFs and CCP stacking of the radial PRFs. The good quality digital waveform of forty-nine good teleseismic events from the 10-station Hyderabad network during 2020–2021 has enabled us to carry out the present study. The analysis of individual, stacked and gather radial PRFs at ten broadband stations depicts that the mean depth to the Moho, Hale's discontinuity and LAB below the study region are modelled to be 36, 115 and 160 km, respectively, which are found to be in a good agreement with the existing estimates of these depths from other studies. We also observe clear conversions from the upper and lower boundaries of the Mantle transition zone (MTZ) on the radial PRFs at all the stations.

The 2-D images generated by our CCP stacking of radial PRFs along four profiles detect five major discontinuities below the region viz. Moho (increase in positive PRF amplitude at 30–40 km depths), Hales discontinuity (increase in positive PRF amplitude at 90–125 km depths), LAB (increase in negative PRF amplitude at 130–160 km depths), 410-km (increase in positive PRF amplitude at 410–440 km

depths) and 660-km (increase in positive PRF amplitude at 620–660 km depths). We also model that the differential time of the 410-km and 660-km conversions at most of the stations is found to be 24 s, which is the same as the theoretical differential time between these two phases according to the IASP91 global reference velocity model. This observation suggests that variations in 410-km and 660-km boundaries are not significant below the region, which is in agreement with the cratonic behaviour of the EDC. However, we notice a marked upward movement of the 410-km boundary and a slight downward movement of 660-km boundary below the central part of the study region, suggesting a alight thickening of the MHT, which could be attributed to the presence of probable imprints of Archean subduction as also suggested by the petrochemical studies of the Hyderabad granites. Our modelling also suggests a lithospheric thickness of 140–160 km, which, in turn, indicates the absence of a thick cratonic lithospheric root (> 250 km thick) below the EDC.

Declarations

Acknowledgements

Authors are grateful to the Director, Council of Scientific and Industrial Research - National Geophysical Research Institute (CSIR-NGRI), Hyderabad, India, for his support and permission to publish this work. Authors are thankful to Dr. Eagar for sharing the Funclab software. Figures were plotted using the Generic Mapping Tool (GMT) software (Wessel et al., 2019; https://doi.org/10.1029/2019GC008515). The elevation data used in generating GMT plots are obtained from the open source Digital Elevation Model (DEM) (https://asterweb.jpl.nasa.gov/gdem.asp).

Funding: Funding was provided by the Council of Scientific and Industrial Research, India (Grant Number: MLP-6401-28(PM))

Competing interests: The authors declare no competing interests.

Data availability

Datasets for the present study are included in this paper and its supplementary information files. Data can also be obtained by sending the email-request to director@ngri.res.in or the corresponding author.

References

1. Berteusen, K. A. (1977). Moho depth determinations based on spectral-ratio analysis of NORSAR long-period P waves. *Phys. Earth Planet. Int.*, 31, 313–326.
2. Bina, C. R. (1991). Mantle Discontinuities. *Reviews of Geophysics*, 29(S2), 783-793. https://doi.org/10.1002/rog.1991.29.s2.783.
3. Borah, K., Kanna, N., Rai, S.S., & Prakasam, K. (2015). Sediment thickness beneath the Indo-gangetic plain and Siwalik Himalaya inferred from receiver function modelling. *Journal of Asian Earth Science*, 99, 41–56. https://doi.org/10.1016/j.jseaes.2014.12.010.

4. Caldwell, W.B., Klemperer, S.L., Lawrence, J.F., Rai, S.S., & Ashis (2013). Characterizing .the Main Himalayan Thrust in the Garhwal Himalaya, India with receiver function CCP stacking. *Ear. Planet. Sci. Lett.*, 367, 15-27.
5. Chevrot, S., Vinnik, L., & Montagner, J-P. (1999). Global-scale analysis of the mantle Pds phases. *Jou. of Geophys. Res. Atm.*, 1042(B9), 20203-20220.
6. Dueker, K.G., & Sheehan, A.F. (1997). Mantle discontinuity structure from midpoint stacks of converted P to S waves across the Yellowstone hotspot track. *J.Geophys. Res.*, 102 (B4), 8313–8327, URL http://dx.doi.org/10.1029/96JB03857.
7. Eagar, K.C. (2012). FuncLab: A MATLAB interactive toolbox for handling receiver function datasets. *Seis. Res. Lett.*, 83, doi:10.1785/gssrl.83.3.596.
8. Fischer, K.M., Ford, H.A., Abt, D.A., & Rychert (2010). The Lithosphere-Asthenosphere Boundary. ***Annual Review of Earth and Planetary Sciences*, 38, 551-575.** https://doi.org/10.1146/annurev-earth-040809-152438
9. Ganguly, J., & Bhattacharya, P.K. (1987). Xenoliths in Proterozoic kimberlites from southern India: petrology and geophysical implications. *Nuclear Physics A*, 0375-9474, 249-265.
10. Gaur, V.K., & Priestley, K. (1997). Shear wave velocity structure beneath the Achaean granites around Hyderabad, inferred from receiver function analysis. *Proc. Indian Acad. Sci (Earth Planet. Sci.)*, 106, 1–8.
11. Gokarn, S.G., Gupta, G., & Rao, C.K. (2004). Geoelectric structure of the Dharwar craton from magnetotelluric studies: Archean suture identified along the Chitradurga-Gadag schist belt. *Geophys. J. Int.*, 158, 712– 728, doi:10.1111/j.1365-246X.2004.02279.x.
12. Griffin, W.L., O'Reilly, S.Y., Afonso, J.C., & Begg, G.C. (2009). The Composition and Evolution of Lithospheric Mantle: a Re-evaluation and its Tectonic Implications. *Journal of Petrology*, 50, 1185–1204, https://doi.org/10.1093/petrology/egn033
13. Gupta, M.L., Sundar, A., & Sharma, S.R. (1991). Heat flow and heat generation in the Archaean Dharwar cratons and implications for the Southern Indian Shield geotherm and lithospheric thickness. *Tectonophysics*, 194, 107-122.
14. Gupta, S., Rai, S.S., Prakasam, K.S., Srinagesh, D., Bansal, B.K., Chadha, R.K., Priestley, K., & Gaur, V.K. (2003). The nature of the crust in south-ern India —implications for Precambrian crustal evolution. *Geophys. Res. Lett.*, 30, 1419, doi:10.1029/2002GL016770
15. Hales, A. (1969). A seismic discontinuity in the lithosphere. *Earth Planet. Sci. Lett.*, 7, 44–46. http://dx.doi.org/10.1016/0012-821X(69)90009-0.
16. Jagadeesh, S., & Rai, S.S. (2008). Thickness, composition, and evolution of the Indian Precambrian crust inferred from broadband seismological measurements. *Precambrian Res.*, 162, 4–15. http://dx.doi.org/10.1016/j.precamres.2007.07.009.
17. Kennett, B.L.N., & Engdahl, E.R. (1991). Travel times for global earthquake location and phase identification. *Geophys. J. Int.*, 105, 429–465, doi 10.1111/j.1365-246X.1991.tb06724.x.

18. Kiselev, S., Vinnik, L., Oreshin, S., Gupta, S., Rai, S.S., Singh, A., Kumar, M.R., & Mohan, G. (2008). Lithosphere of the Dharwar craton by joint inversion of P and S receiver functions. *Geophysical Journal International*, 173, 1106-1118.
19. Kumar, M.R., Saul, J., Sarkar, D., Kind, R., & Shukla, A.K. (2001). Crustal structure of the Indian shield: New constraints from teleseismic receiver functions. *Geophysical Research Letters*, 28(7), 1339–1342. https://doi.org/10.1029/2000GL012310.
20. Kumar, M.R., & Mohan, G. (2005). Mantle discontinuities beneath the Deccan volcanic province. *Earth and Planetary Science Letters*, 237, 252-263.
21. Kumar, P., Yuan, X., Kumar, M.R., Kind, R., Li, X., & Chadha, R.K. (2007). The rapid drift of the Indian tectonic plate. *Nature*, 449, 894–897. http://dx.doi.org/10.1038/ nature06214.
22. Ligorria, J.P., & Ammon, C.J. (1999). Iterative deconvolution and receiver function estimation. *Bulletin of the Seismological Society of America*, 89, 1395–1400.
23. *Lowrie, W. (1997).* Fundamentals of Geophysics*.* Cambridge University Press*. p. 149.* ISBN 9780521467285.
24. Mandal, P., Saha, S., Kumar, S., Gupta, S., Biswas, R., Kumar, S., Sivaram, K., Prasad, B.N.V., Saidixit, M., Prathigadapa, R., Singh, B., & Madhusudan, S. (2022). Modelling of Moment Tensors and Source Parameters of the 25 July 2021 Rare Lower Crustal Hyderabad (India) Earthquake of M_w 3.9. *Pure Appl. Geophys.*, 179, 993-1010. https://doi.org/10.1007/s00024-022-02973-6.
25. Naganjaneyulu, K., & Santosh, M. (2011). Crustal architecture beneath Madurai Block, southern India deduced from magnetotelluric studies: Implications for subduction–accretion tectonics associated with Gondwana assembly. *Journal of Asian Earth Sciences*, 40, 132-143. 10.1016/j.jseaes.2010.08.014.
26. Negi, J., Pandey, O.P., & Agrawal, P.K. (1986). Super-mobility of hot Indian lithosphere. *Tectonophysics*, 131, 147–156. http://dx.doi.org/10.1016/0040-1951(86)90272-6.
27. O'Reilly, S., & Griffin, W. (2013). Moho vs crust–mantle boundary: Evolution of an idea. *Tectonophysics*, 609. 535–546. 10.1016/j.tecto.2012.12.031.
28. Ottemoller, L., Voss, P., & Havskov, J. (2018). Seisan Earthquake Analysis Software, Version 11.
29. Pahari, A., Prasanth, P., Tiwari, D., Manikyamba, C., & Subramanyam, K.S.V. (2020). Subduction–collision processes and crustal growth in eastern Dharwar Craton: Evidence from petrochemical studies of Hyderabad granites. *Jou. Ear. Syst. Sci.*, 129, 1-21.
30. Pandey, O.P., & Agarwal, P.K. (1999). Lihtospheric mantle Deformation beneath the Indian Cratons. *The Journal of Geology*, 107, 683-692.
31. Patro, P.K., & Sarma, S.V.S. (2009). Lithospheric electrical imaging of the Deccan trap covered region of western India. *Journal ofGeophysical Research,* 114, B01102, doi:10.1029/2007JB005572.
32. Polet, J., & Anderson, D.L. (1995). Depth extent of cratons as inferred from tomographic studies. *Geology*, 23(3), 205–208.

33. Rai, S.S., Priestley, K., Suryaprakasam, K., Srinagesh, D., Gaur, V.K., & Du, Z. (2003). Crustal shear velocity structure of the south Indian shield. *J. Geophys. Res.*, 108(B2), 2088, doi:10.1029/2002JB001776.
34. Ramesh, D.S., Bianchi, M.B., & Das Sharma, S. (2010). Images of possible fossil collision structures beneath the Eastern Ghats belt, India, from P and S receiver functions. *Lithosphere*, 2(2), 84-92.
35. Rychert, C.A., & Harmon, N. (2016). Stacked P-to-S and S-to-P receiver functions determination of crustal thickness, Vp, and Vs: The H-V stacking method. *Geophys. Res. Lett.*, 43, 1487–1494, doi:10.1002/2015GL067010.
36. Saha, G.K., Prakasam, K.S., & Rai, S.S. (2020). Diversity in the peninsular Indian lithosphere revealed from ambient noise and earthquake tomography. *Phys, Earth and Planet. Interiors*, 306, 106523, 1–17.
37. Sarkar, D., Ravikumar, M., Saul, J., Kind, R., Raju, P.S., Chadha, R.K., & Shukla, A.K. (2003). A receiver function perspective of the Dharwar craton (India) crustal structure. *Geophys. Jour. Int.*, 154, 205-211.
38. Saul, J., Ravikumar, M., & Sarkar, D. (2000). Lithospheric and upper mantle structure of the Indian shield from teleseismic receiver functions. *Geophys. Res. Lett.*, 27, 2357- 2360.
39. Shearer, P. M. (2000). Upper mantle seismic discontinuities. *Geophysical Monograph Series*, 117, 115-131. DOI:10.1029/GM117p0115
40. Shearer, P. (2019). Introduction to Seismology (3rd ed.). Cambridge: Cambridge University Press. doi:10.1017/9781316877111
41. Shukla, S., & Ram Mohan, M. (2019). Magma mixing in Neoarchean granite from Nalgonda region, Eastern Dharwar Craton, India: Morphological, mineralogical and geochemical evidences. *J. Earth Syst. Sci.*, 128, 71.
42. Singh, A.P., Vijayakumar, V., & Mishra, D.C. (2004). Subsurface geometry of Hyderabad granite pluton from gravity and magnetic anomalies and its role in the seismicity around Hyderabad. *Curr. Sci.*, 86(4), 580-586.
43. Singh, A., Singh, C., & Kennett, B.L.N. (2015). A review of crust and upper mantle structure beneath the Indian subcontinent. *Tectonphysics*, 644/645, 1-21.
44. Srinagesh, D., Rai, S.S., Ramesh, D.S., Gaur, V.K., & Rao, C.V. (1989). Evidence for thick continental roots beneath south Indian shield. *Geophysical Research Letters*, 6, 1055-1058.,
45. Wessel, P., Luis, J. F., Ujeda, L., Scharroo, R., Wobbe, F., Smith, W. H. F., et al. (2019). Generic Mapping Tools version 6. Geochemistry, Geophysics, Geosystems, 20, 5556–5564. https://doi.org/10.1029/2019GC008515
46. Zhou, L., Chen, W. –P., & Ozalaybey, S. (2000). Seismic properties of central Indian shield. *Bull. Seism. Soc. Amer.*, 90, 1295-1304.

Tables

Table 1 is not available with this version

Figures

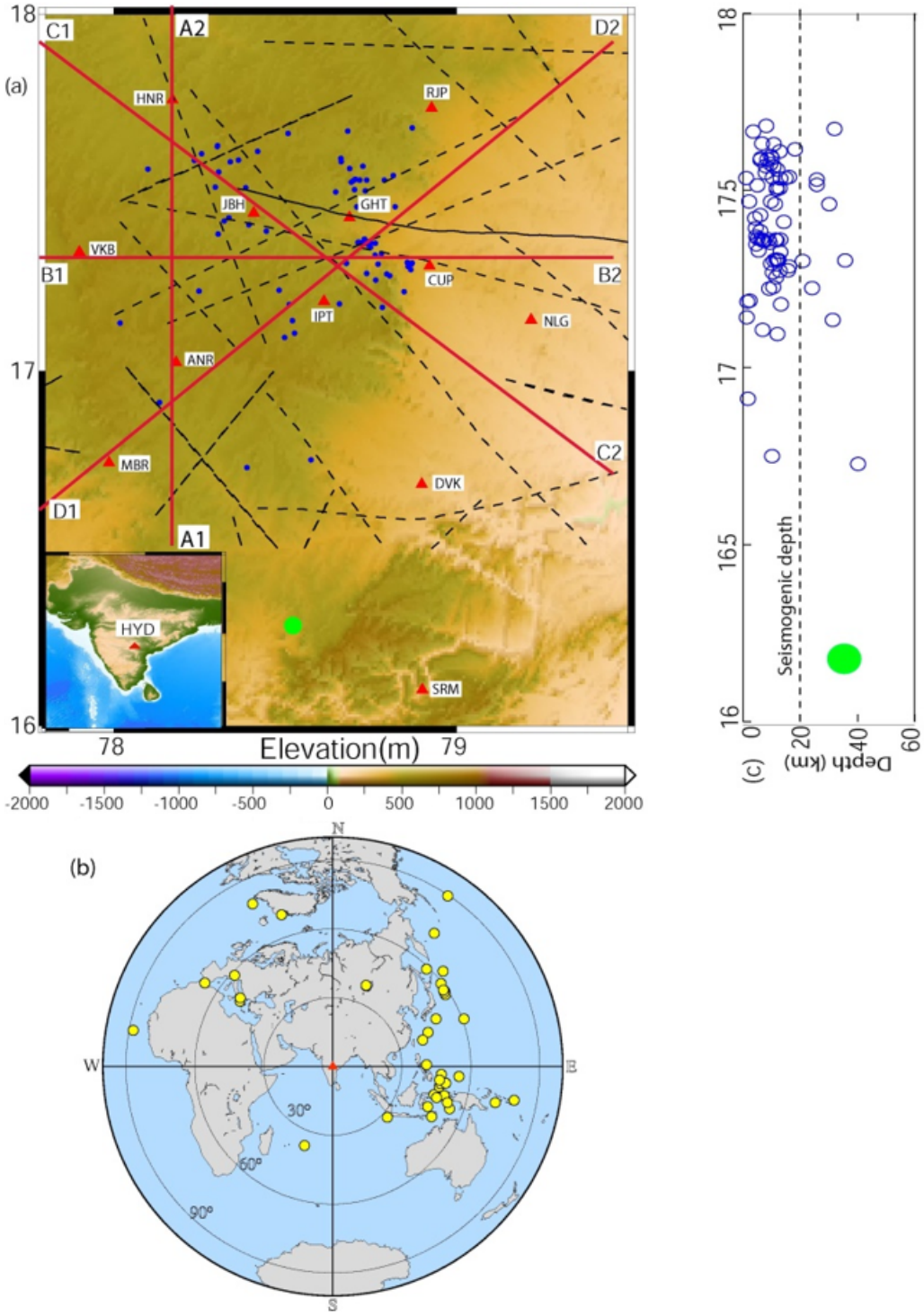

Figure 1

(a) Elevation map of the Hyderabad region, India, showing the newly installed seismic network of 10 broadband stations. Red filled triangles mark the broadband stations. Small blue filled circles mark the locations of micro-earthquakes (during 2020-21). Black dotted lines mark faults and lineaments in the area. Large green filled circle marks the location of July 2021 event of M_w3.9. Locations of 4 profiles (A1A2, B1B2, C1C2 and D1D2) across the study area are shown by solid red lines, (b) Depth sections of micro-seismicity in Hyderabad during Sept. 2020 – August 2021, and (c) Epicentral locations (marked by filled yellow circles) of 49 teleseismic events, whose waveforms are used for the PRF computation. A filled red triangle marks the center of the seismic network.

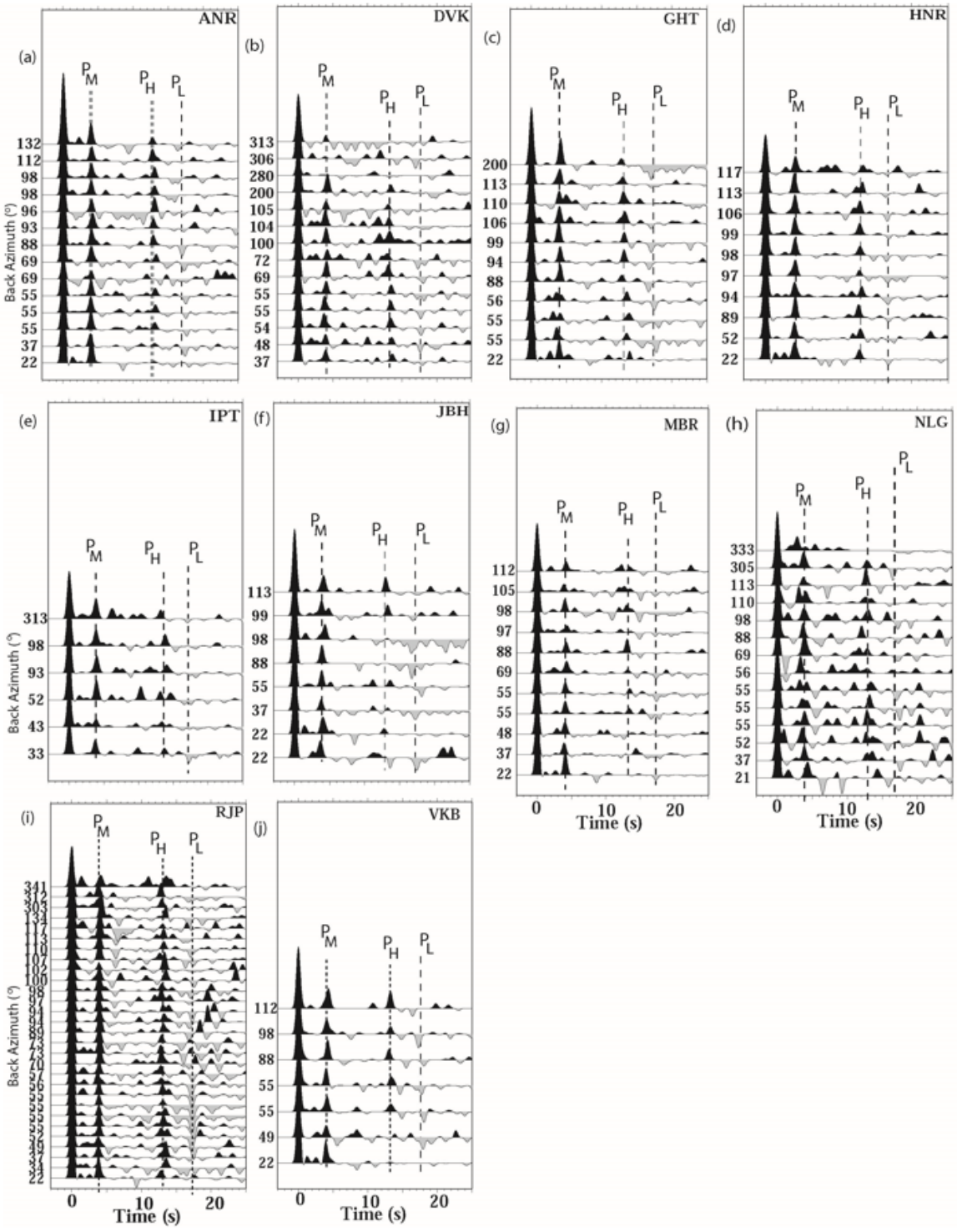

Figure 2

Radial PRFs estimated for Gaussian width (a) =2.5 stored according to slowness for stations, (a) ANR, (b) DVK. (c) GHT, (d) HNR, (e) IPT, (f) JBH, (g) MBR, (h) NLG, (i) RJP and (j) VKB. Grey dotted lines mark the Moho conversion (P_M), Conversion from Hale's discontinuity (P_H), and Lithosphere-Asthenosphere boundary (LAB) conversion (P_L).

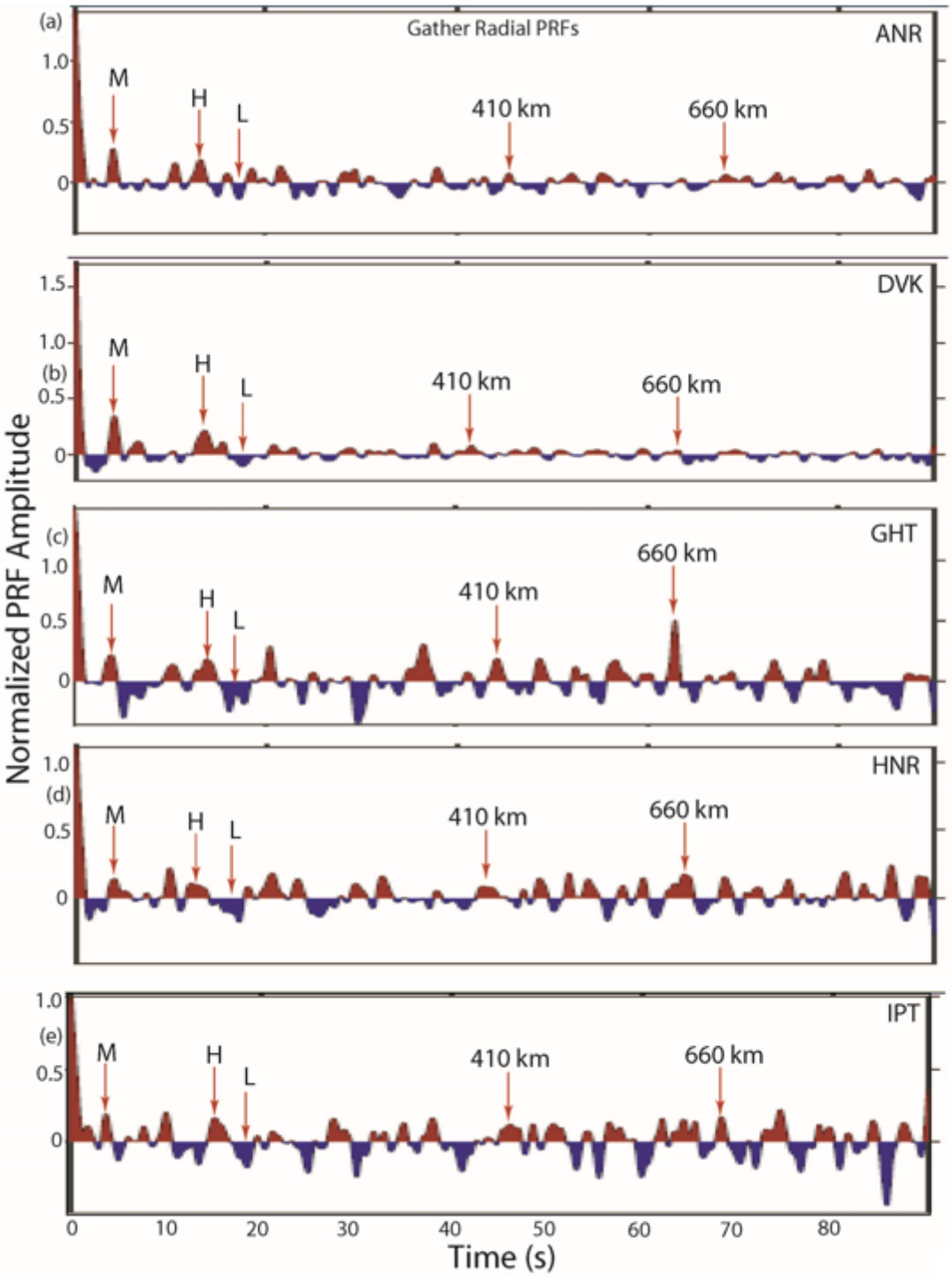

Figure 3

Gather radial PRFs at different stations viz., (a) ANR, (b) DVK, (c) GHT, (d) HNR and (e) IPT, showing P-to-S conversions from Moho (M), Hale's (H), LAB (L), 410 km and 660 km discontinuities.

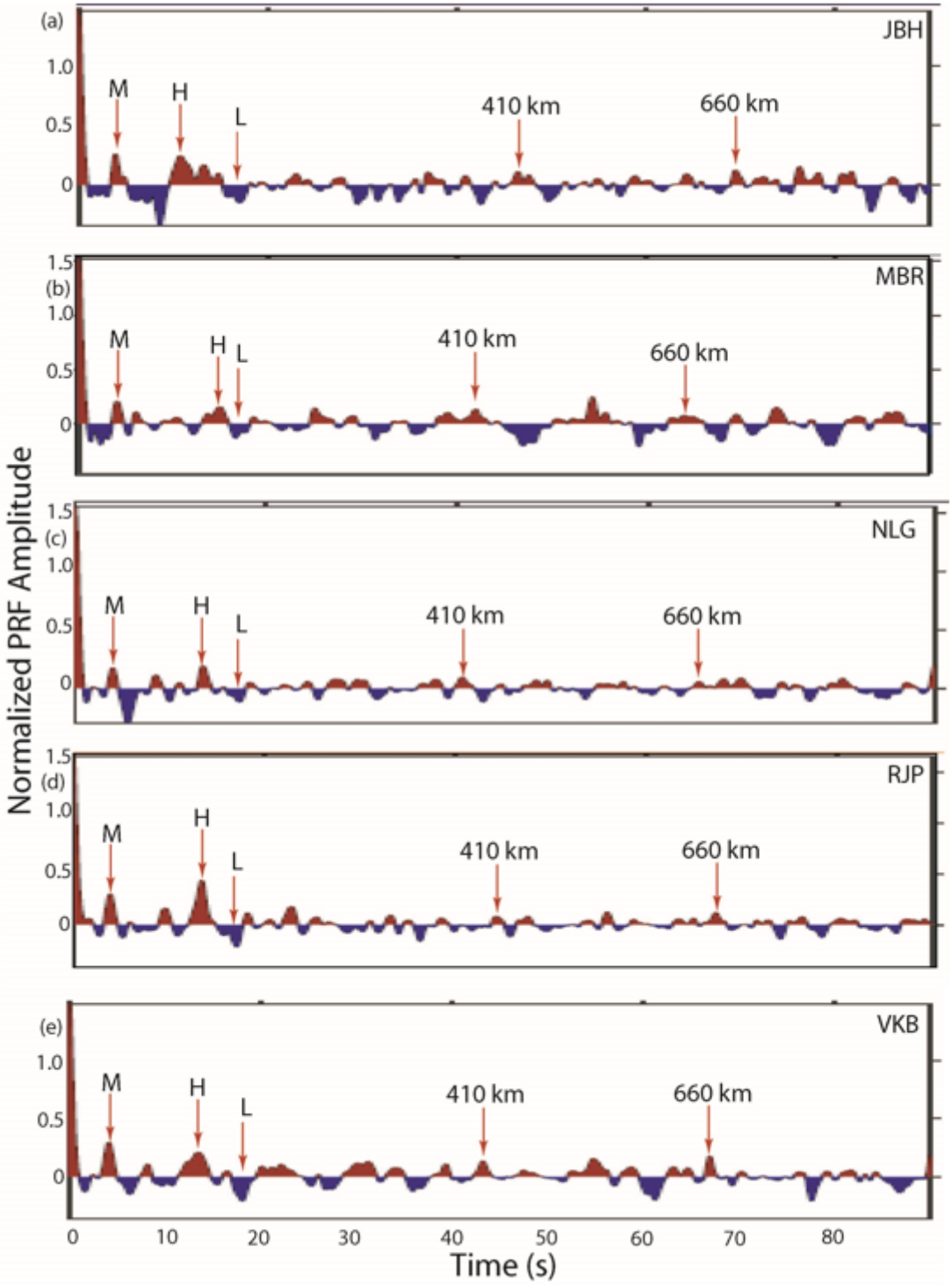

Figure 4

Gather radial PRFs at different stations viz., (a) JBH, (b) MBR, (c) NLG, (d) RJP and (e) VKB, showing P-to-S conversions from Moho (M), Hale's (H), LAB (L), 410 km and 660 km discontinuities.

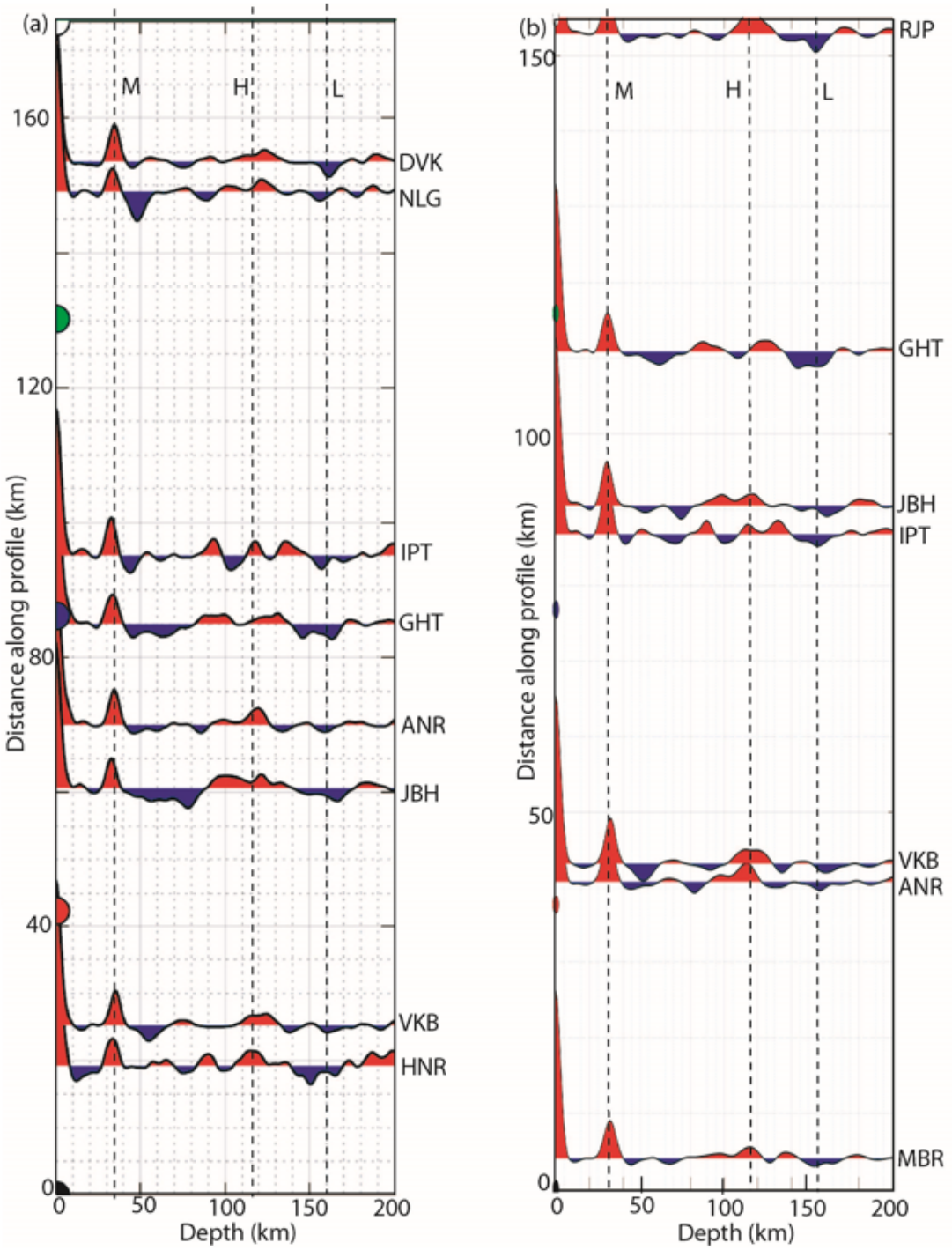

Figure 5

Depth-wise migrated stacked radial PRFs (a) at eight stations (namely, DVK, NLG, IPT, GHT, ANR, JBH, VKB and HNR) and (b) at seven stations (RJP, GHT, IPT, VKB, ANR and MBR), showing positive arrivals from the Moho and Hale's discontinuities and negative arrivals from the lithosphere-asthenosphere boundary (marked by grey dotted lines).

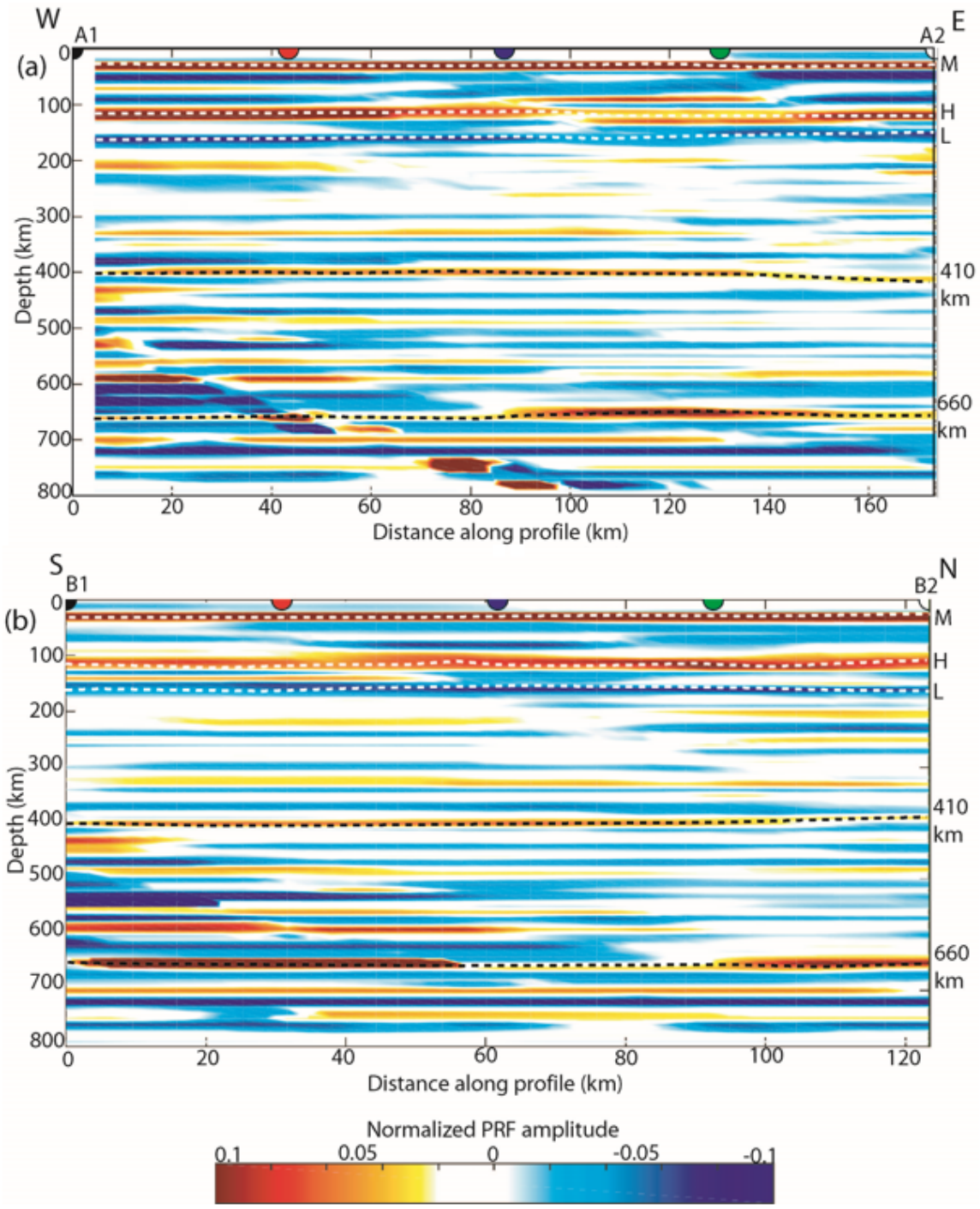

Figure 6

CCP stacking of radial PRFs along the (a) WE and (b) SN profiles, showing crustal and mantle discontinuities. White dotted lines mark variations in the Moho depth, Hale's discontinuity and

lithosphere-asthenosphere boundary across the Hyderabad region. While black dotted lines mark the upper and bottom layer of the Mantle transition zone (at 410 km and 660 km depths).

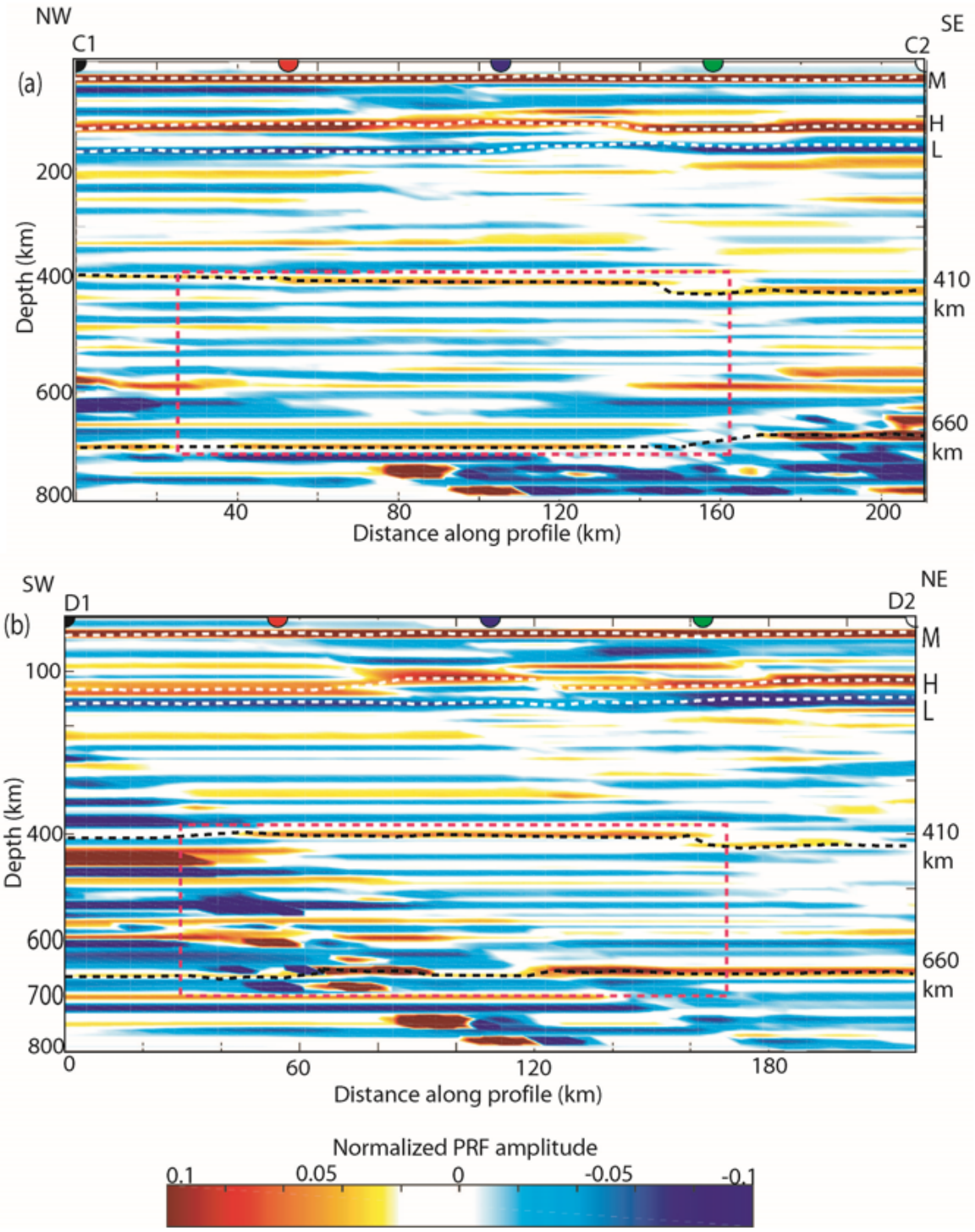

Figure 7

Similar to the Figure 6 across the profile (a) NW-SE and (b) SW-NE. The dotted red rectangular are marks the maximum deformed zone of the MTZ below the region, suggesting a thickening of the MTZ at the central portion of the SW-NE and NW-SE profiles.

Supplementary Files

This is a list of supplementary files associated with this preprint. Click to download.

- supplimentaryinformation.docx